REVIEW

The dynamics of some exact solutions of the (3+1)-dimensional generalized shallow water wave equation

Lingna Ying · Maohua Li

Abstract The (3+1)-dimensional generalized shallow water wave equation is systematically investigated in this paper based on the Hirota bilinear method. The N-soliton solution and the higher-order kink-shaped breather solutions of the (3+1)-dimensional generalized shallow water wave equation are first proposed. Then, the line rogue wave solution and various hybrid solutions consisting of the breather, the kink-shaped soliton and the periodic solutions are discussed. Furthermore, the lump solutions of it are derived by using the long wave limit of the N-soliton solution. In addition, the diverse semi-rational solutions composed of lumps, kink solitons, line rogue wave and breathers enrich the research contents of the (3+1)-dimensional generalized shallow water wave equation. The dynamic behaviors of these exact solutions are vividly presented by their respective three-dimensional diagrams and density plots with contours.

L. Ying · M. Li (✉)
School of Mathematics and Statistics, Ningbo University, Ningbo 315211, Zhejiang, People's Republic of China
e-mail: limaohua@mail.ustc.edu.cn

1 Introduction

As significant mathematical models capable of describing some nonlinear phenomena, nonlinear evolution equations (NLEEs) have always been highly valued by scholars in mathematics, physics and even engineering due to their important statuses in such scientific fields as plasma physics, optical fiber communication, nonlinear atmospheric dynamics, quantum mechanics, etc. Meanwhile, the solutions to the emerging nonlinear evolution equations with nonlinear dispersion and dissipation effects are the subjects that the majority of nonlinear scientific researchers have to consider. Soliton refers to the solution with particle structural state of a class of nonlinear dispersion equations [1]. Soliton, chaos and fractal constitute the three major theories of nonlinear science, which respectively represent the three universal classes of nonlinear phenomena. The kinematic mechanism of solitons and waves has become an important research field that is active internationally since the numerical research results of the famous nonlinear shallow water wave Korteweg-de Vries (KdV) equation were published by Zabusky and Kruskal [2]. A series of methods for solving nonlinear evolution equations emerged as the times require in the theory of soliton and integrable system, such as the inverse scattering transformation (IST) [3–5], the homogeneous balance method [6,7], the function expansion method [8,9], the Bäcklund transformation (BT) [10–12], the Darboux transformation (DT) [13–

15] and the Hirota bilinear method [16–19]. Among them, the Hirota bilinear method is highlighted as a powerful weapon that was first proposed by Ryogo Hirota [16], to find the exact solutions of various nonlinear evolution equations. Some popular integrable equations such as the Kadomtsev-Petviashvili (KP) equation [20–22] and the Davey-Stewartson (DS) equation [23,24] have been studied in detail based on these methods.

The types of exact solutions are also rich and varied, including the bright solitons, the dark solitons, the kink solitons, the breathers, the rogue waves, and the lumps [25–35]. Due to the combined effect of nonlinearity and dispersion, the soliton solution keeps its original stable wave packet characteristics during nonlinear wave propagation and after collision, which undoubtedly shows the amazing orderliness caused by nonlinear effects [1,2,25–27]. The breathers oscillate periodically in a certain region of the finite background during transmission [29–31]. In particular, the rogue waves and the lump solutions, as rational function solutions of nonlinear wave equations, have increasingly become the focus of attention due to their special structures and potential destructiveness [31–35]. The rogue waves were first proposed when Peregrine studied the general nonlinear Schrödinger (NLS) equation [36] and often "come without shadow and go without trace" [37], which are interpreted as the phenomena of energy concentration in the nonlinear theory. Their peak amplitudes are usually about three times of the background waves, and they will eventually attenuate to a constant background wave. The rogue wave phenomena also exist in such fields as oceanography, optics, Bose Einstein condensate, plasma physics, atmospheric science, etc [38–43].

However, since most of the rogue wave phenomena in the ocean are described by (2+1)- or (3+1)-dimensional models, and the research on low-dimensional nonlinear models has been relatively mature [30–34,38], the research on (3+1)- and even higher-dimensional nonlinear models has become necessary. For example, the algebraic-geometrical solutions, N-soliton solution and its Wronskian form of a (3+1)-dimensional nonlinear evolution equation are solved in detail [44,45]. The solitary wave solutions, lump-type solutions, and rogue wave solutions of the (3+1)-dimensional Jimbo-Miwa equation have been studied [46–48]. And the multiple-soliton solutions, multiple singular soliton solutions, Wronskian and Grammian solutions of a (3+1)-dimensional generalized Kadomtsev-Petviashvili (KP) equation are constructed [49–51].

This paper focuses on a (3+1)-dimensional nonlinear model, namely the (3+1)-dimensional generalized shallow water wave (gSWW) equation as

$$(u_t + u_{xxx})_y - 3(u_x u_y)_x + u_{xz} = 0, \tag{1.1}$$

where $u = u(x, y, z, t)$, which can be equivalent to the general expression of the (3+1)-dimensional generalized shallow water wave (gSWW) equation [52–56]

$$u_{yt} + u_{xxxy} - 3u_{xx}u_y - 3u_x u_{xy} - u_{xz} = 0, \tag{1.2}$$

under a scale transformation $z \rightarrow -z$. Tian et al. have obtained the soliton-typed solutions of the (3+1)-dimensional gSWW equation by using the tanh function method with symbolic computation [54]. Three functional representations of the traveling wave solutions of the equation have been derived by Zayed through the $(\frac{G'}{G})$-expansion method [55]. Based on the Hirota bilinear method, Tang and Ma et al. calculated the solutions of the equation in Grammian and Pfaffian forms [56]. Some singular soliton solutions, hyperbolic function solutions and trigonometric function solutions of the equation are proposed by Zeng and Liu et al. through the Painlevé Bäcklund transformation and the Hirota bilinear method [57]. Liu et al. used the auto-Bäcklund transformation and a direct test function to obtain some periodic solitary wave solutions for the equation [58]. And Eq. (1.1) describes the propagation of shallow water waves in oceans, estuaries and reservoirs, and can be applied to weather simulation, tidal waves, rivers and irrigation flows, tsunami forecasts, etc. As we know, the higher-order kink-shaped soliton and breather solutions, the rogue wave (RW) solutions, the RW-soliton and lump-breather semi-rational solutions, and the hybrid solutions composed of different solutions of Eq. (1.1) are still to be explored. As a consequence, this paper focuses on the dynamic behaviors of new exact solutions of Eq. (1.1) heartened by the above open problems, and hopes to learn more about the new characteristics of Eq. (1.1) during the research.

The main structure of this paper is as follows. In Sect. 2, based on the Hirota bilinear method combined with a logarithmic transformation and the perturbation method, the explicit expression of the N-soliton solution and the kink-shaped multi-soliton solutions of Eq. (1.1) are derived. In Sect. 3, the higher-order breather solutions and the hybrid solutions of Eq. (1.1)

are constructed under special constraints of parameters. In Sect. 4, the lump solutions and the line rogue wave solution of Eq. (1.1) are generated by taking the long wave limit [59–63]. In Sect. 5, various types of semi-rational solutions of Eq. (1.1) are explored. The conclusion of this paper is given in Sect. 6.

2 The bilinear form and the soliton solutions of the (3+1)-dimensional gsww equation

In order to obtain the Hirota bilinear form of Eq. (1.1), a binary differential D-operator (i.e. the Hirota derivative) [18] is introduced as

$$
\begin{aligned}
D_x^n a(x) \cdot b(x) &\equiv \left(\frac{\partial}{\partial x} - \frac{\partial}{\partial y}\right)^n a(x)b(y)|_{y=x} \\
&= \frac{\partial^n}{\partial y^n} a(x+y)b(x-y)|_{y=0},
\end{aligned}
\tag{2.1}
$$

$$
\begin{aligned}
D_t^m D_x^n a(t, x) \cdot b(t, x) &\equiv \frac{\partial^m}{\partial s^m} \frac{\partial^n}{\partial y^n} a(t+s, x+y) \\
&\quad b(t-s, x-y)|_{s=0, y=0},
\end{aligned}
\tag{2.2}
$$

where m and n are arbitrary non-negative integers. By performing a corresponding logarithmic transformation on u

$$
u = -2(\ln f)_x,
\tag{2.3}
$$

Eq. (1.1) can be transformed into a bilinear derivative equation

$$
(D_t D_y + D_x^3 D_y + D_x D_z)f \cdot f = 0.
\tag{2.4}
$$

This is equivalent to the bilinear expansion of Eq. (1.1), written as follows

$$
\begin{aligned}
&ff_{ty} - f_t f_y + ff_{xxxy} - f_{xxx}f_y - 3f_{xxy}f_x \\
&+ 3f_{xx}f_{xy} + ff_{xz} - f_x f_z = 0,
\end{aligned}
\tag{2.5}
$$

where $f = f(x, y, z, t)$.

By using the standard perturbation method to solve Eq. (2.4), $f(x, y, z, t)$ is expanded into a power series according to the small parameter ε

$$
f(x, y, z, t) = 1 + \varepsilon f_1 + \varepsilon^2 f_2 + \cdots + \varepsilon^j f_j + \cdots.
\tag{2.6}
$$

After substituting it into Eq. (2.4), it can be rearranged by comparing the coefficients of the same power of ε, then

$$
\varepsilon : f_{1,ty} + f_{1,xxxy} + f_{1,xz} = 0,
\tag{2.7a}
$$

$$
\begin{aligned}
\varepsilon^2 &: 2(f_{2,ty} + f_{2,xxxy} + f_{2,xz}) \\
&= -(D_t D_y + D_x^3 D_y + D_x D_z)f_1 \cdot f_1,
\end{aligned}
\tag{2.7b}
$$

$$
\begin{aligned}
\varepsilon^3 &: f_{3,ty} + f_{3,xxxy} + f_{3,xz} \\
&= -(D_t D_y + D_x^3 D_y + D_x D_z)f_1 \cdot f_2,
\end{aligned}
\tag{2.7c}
$$

$$
\begin{aligned}
\varepsilon^4 &: 2(f_{4,ty} + f_{4,xxxy} + f_{4,xz}) \\
&= -(D_t D_y + D_x^3 D_y + D_x D_z)(2f_1 \cdot f_3 + f_2 \cdot f_2),
\end{aligned}
\tag{2.7d}
$$
$\cdots$.

The power series (2.6) can be truncated at the sum of finite terms while properly selecting the solution f_1 in the form of a linear exponential function under the conditions of the above equations, hence,

$$
f(x, y, z, t) = 1 + \varepsilon f_1 = 1 + \varepsilon e^{\eta_1},
\tag{2.8}
$$

where

$$
\begin{aligned}
\eta_1 &= p_1 x + q_1 y + k_1 z + \omega_1 t + \eta_1^0, \\
\omega_1 &= -\frac{p_1(p_1^2 q_1 + k_1)}{q_1}.
\end{aligned}
\tag{2.9}
$$

Since the perturbation parameter ε can be absorbed by the phase constant η_1^0 of the exponent η_1, the exact solution of Eq. (2.4) is given as follows

$$
f(x, y, z, t) = 1 + e^{\eta_1}.
\tag{2.10}
$$

Further, combining the transformation (2.3), the single solitary wave solution u_{1s} of Eq. (1.1) is obtained as

$$
u_{1s} = -\frac{2p_1}{1 + e^{-(p_1 x + q_1 y + k_1 z + \omega_1 t + \eta_1^0)}}.
\tag{2.11}
$$

Note that the arbitrary parameter η_1^0 in this expression represents the position of the soliton, which is typically taken as 0. In addition, the 1-soliton solution u_{1s} has no extreme point, showing the following characteristics:

$$
\begin{cases}
u_{1s} \to -2p_1 & \text{for } \eta_1 \to +\infty \\
u_{1s} \to 0 & \text{for } \eta_1 \to -\infty
\end{cases}.
\tag{2.12}
$$

In the asymptotic dynamic behavior of the 1-soliton solution u_{1s}, u_{1s} will degenerate into a plane wave when $p_1 = 0$, otherwise u_{1s} will degenerate into a kink wave. When all the parameters in (2.11) are assigned specific values, the 1-kink soliton solution of Eq. (1.1) is shown in Fig. 1.

Since Eq. (2.7a) is a linear differential equation, a superposition solution of it can be given by applying the linear superposition principle

$$
\begin{aligned}
f_1 &= e^{\eta_1} + e^{\eta_2}, \quad \eta_i = p_i x + q_i y + k_i z + \omega_i t + \eta_i^0, \\
\omega_i &= -\frac{p_i(p_i^2 q_i + k_i)}{q_i} \quad (i = 1, 2).
\end{aligned}
\tag{2.13}
$$

Fig. 1 The 1-kink soliton solution of Eq. (1.1) in the (x, y)-plane at $t = 0$ with parameters: $N = 1$, $p_1 = q_1 = k_1 = -1$, $\eta_1^0 = 0$. **a** The 3D plot. **b** The density plot. (Color online)

(a) $t = 0$

(b) $t = 0$
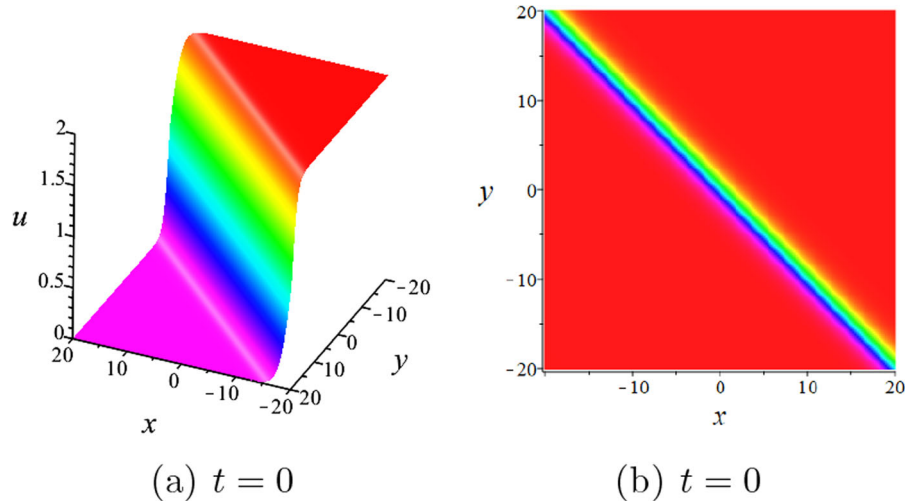
After substituting (2.13) into Eq. (2.7b), the following will be obtained

$$f_2 = e^{\eta_1 + \eta_2 + A_{12}}, \tag{2.14}$$

where

$$\eta_i = p_i x + q_i y + k_i z + \omega_i t + \eta_i^0,$$
$$\omega_i = -\frac{p_i(p_i^2 q_i + k_i)}{q_i} \quad (i = 1, 2, 3) \tag{2.19}$$

$$e^{A_{12}} = \frac{p_2 q_1^2(3 p_1 q_2(p_1 - p_2) - k_2) - q_1 q_2(3 p_1 p_2 q_2(p_1 - p_2) - p_1 k_2 - p_2 k_1) - p_1 q_2^2 k_1}{p_2 q_1^2(3 p_1 q_2(p_1 + p_2) - k_2) + q_1 q_2(3 p_1 p_2 q_2(p_1 + p_2) + p_1 k_2 + p_2 k_1) - p_1 q_2^2 k_1}. \tag{2.15}$$

Then, by continuing to apply the perturbation method, the truncated solution of Eq. (2.4) will be transformed into

$$f(x, y, z, t) = 1 + e^{\eta_1} + e^{\eta_2} + e^{\eta_1 + \eta_2 + A_{12}}. \tag{2.16}$$

Thus, combining the transformation (2.3), the 2-soliton solution of Eq. (1.1) is solved as

$$u_{2s} = -2[\ln(1 + e^{\eta_1} + e^{\eta_2} + e^{\eta_1 + \eta_2 + A_{12}})]_x, \tag{2.17}$$

where η_i $(i = 1, 2)$ and $e^{A_{12}}$ are given in (2.13), (2.15). Under the condition that the phase constants η_i^0 $(i = 1, 2)$ are assigned as 0, the interactions between two kink-shaped solitons in two different cases are described (see Fig. 2a, b, e and f).

The method similar to the previous one is adopted to explain that Eq. (1.1) has the 3-soliton solution as follows

$$u_{3s} = -2[\ln(1 + e^{\eta_1} + e^{\eta_2} + e^{\eta_3} + e^{\eta_1 + \eta_2 + A_{12}}$$
$$+ e^{\eta_1 + \eta_3 + A_{13}} + e^{\eta_2 + \eta_3 + A_{23}} \tag{2.18}$$
$$+ e^{\eta_1 + \eta_2 + \eta_3 + A_{12} + A_{13} + A_{23}})]_x,$$

where

$$e^{A_{ij}} = \frac{\begin{aligned}&p_j q_i^2(3 p_i q_j(p_i - p_j) - k_j) - q_i q_j(3 p_i p_j q_j(p_i \\ &\quad - p_j) - p_i k_j - p_j k_i) - p_i q_j^2 k_i\end{aligned}}{\begin{aligned}&p_j q_i^2(3 p_i q_j(p_i + p_j) - k_j) + q_i q_j(3 p_i p_j q_j(p_i \\ &\quad + p_j) + p_i k_j + p_j k_i) - p_i q_j^2 k_i\end{aligned}}$$
$$(i < j, i, j = 1, 2, 3). \tag{2.20}$$

After regulating specific parameters, the 3-kink soliton solution of Eq. (1.1) is shown in Fig. 2c and g. Furthermore, the dynamic behavior of four solitons colliding with each other is also depicted (see Fig. 2d and h).

There is no doubt that the above method for constructing and analyzing the interactions of multi-solitary waves can be completely extended to the case of N-solitary waves. Then the N-soliton solution of Eq. (1.1) can be expressed as follows

$$u = -2(\ln f)_x$$
$$= -2\left[\ln\left(\sum_{\mu = 0, 1} e^{\sum_{i=1}^{N} \mu_i \eta_i + \sum_{1 \le i < j}^{N} \mu_i \mu_j A_{ij}}\right)\right]_x, \tag{2.21}$$

(a) $t = 0$ (b) $t = 0$ (c) $t = 0$ (d) $t = 0$

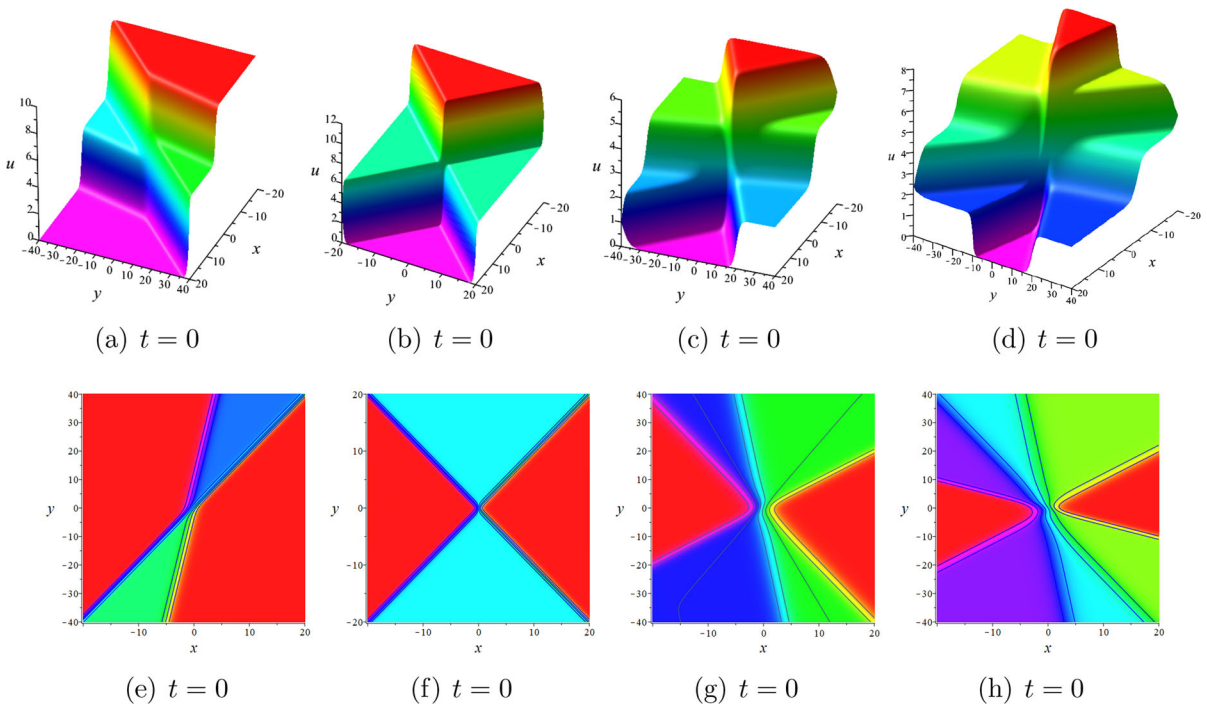(e) $t = 0$ (f) $t = 0$ (g) $t = 0$ (h) $t = 0$

Fig. 2 The 2-, 3-, 4-kink soliton solutions of Eq. (1.1) in the (x, y)-plane at $t = 0$ with parameters: **a**, (e)$N = 2$, $p_1 = -2$, $p_2 = -3$, $q_1 = \frac{1}{4}$, $q_2 = \frac{3}{2}$, $k_1 = k_2 = 1$, $\eta_1^0 = \eta_2^0 = 0$; **b**, (f)$N = 2$, $p_1 = p_2 = q_1 = -q_2 = -3$, $k_1 = k_2 = 1$, $\eta_1^0 = \eta_2^0 = 0$; **c**, (g)$N = 3$, $p_1 = p_2 = p_3 = -1$, $q_1 = -\frac{1}{2}$, $q_2 = 1$, $q_3 = -\frac{1}{9}$, $k_1 = k_2 = k_3 = 2$, $\eta_1^0 = \eta_2^0 = \eta_3^0 = 0$; **d**, (h)$N = 4$, $p_1 = p_2 = p_3 = p_4 = -1$, $q_1 = -\frac{1}{2}$, $q_2 = 1$, $q_3 = -\frac{1}{9}$, $q_4 = -2$, $k_1 = k_2 = k_3 = k_4 = 2$, $\eta_1^0 = \eta_2^0 = \eta_3^0 = \eta_4^0 = 0$. (Color online)

where
$$\eta_i = p_i x + q_i y + k_i z + \omega_i t + \eta_i^0,$$

$$\omega_i = -\frac{p_i(p_i^2 q_i + k_i)}{q_i},$$

$$e^{A_{ij}} = \frac{\begin{aligned}&p_j q_i^2 (3 p_i q_j (p_i - p_j) - k_j) - q_i q_j (3 p_i p_j q_j (p_i\\ &\quad - p_j) - p_i k_j - p_j k_i) - p_i q_j^2 k_i\end{aligned}}{\begin{aligned}&p_j q_i^2 (3 p_i q_j (p_i + p_j) - k_j) + q_i q_j (3 p_i p_j q_j (p_i\\ &\quad + p_j) + p_i k_j + p_j k_i) - p_i q_j^2 k_i\end{aligned}}.$$

$$(2.22)$$

Here, p_i, q_i, k_i and η_i^0 are all arbitrary real or complex parameters, and subscripts i and j denote positive integers. The first summation symbol $\sum_{\mu=0,1}$ behind the logarithmic sign shall take all possible combinations of $\mu_i = 0, 1$ $(i = 1, 2, \cdots, N)$, which represents the addition of 2^N items. The symbol $\sum_{1 \leq i < j}^{N}$ indicates the summation over all possible combinations of the N elements with the specific condition $1 \leq i < j \leq N$. In

addition, the formula $\omega_i + \frac{p_i(p_i^2 q_i + k_i)}{q_i} = 0$ describes the nonlinear dispersion relation of Eq. (1.1). This is the critical factor that affects the periodicity and locality of the energy distribution in other rich solutions of Eq. (1.1).

On the basis of assigning appropriate specific values to the parameters in (2.11), (2.17), (2.18), (2.21), the diagrams of the single soliton and multi-soliton solutions are demonstrated, which show the shape characteristics of kinks. Actually, $p_i \neq 0$ $(i = 1, 2, 3, 4)$ in formula (2.22) are the essence that causes these multisoliton solutions to exhibit kink characteristics, and whether p_i $(i = 1, 2, 3, 4)$ are assigned the same value also implies the diversity of the multi-soliton solutions of Eq. (1.1). The propagations of solitary waves with particle structural state can be observed intuitively from these graphics. Collisions between solitary waves are elastic because of the interaction of dispersion and nonlinear effects, that is, changes in phases are permitted, but the shapes, sizes (velocities) and directions do
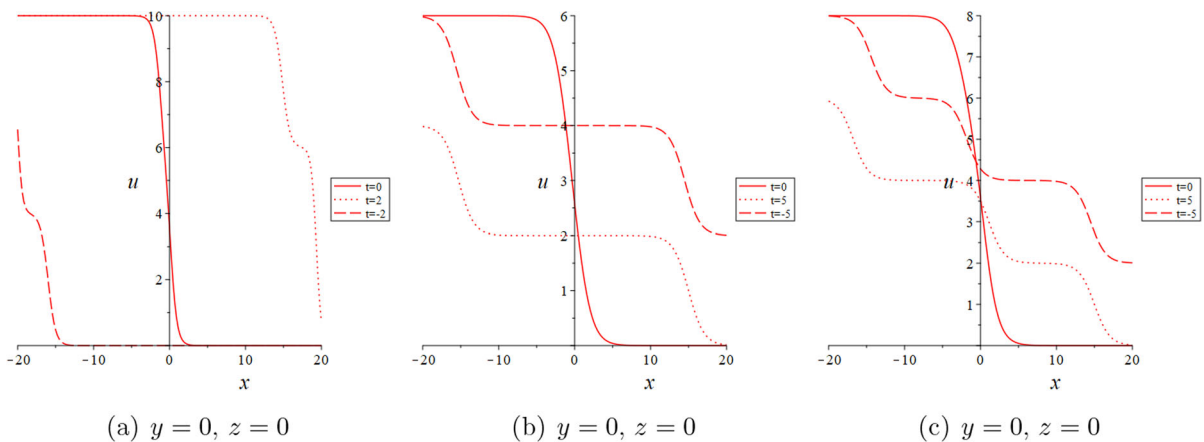
(a) $y = 0$, $z = 0$ (b) $y = 0$, $z = 0$ (c) $y = 0$, $z = 0$

Fig. 3 Sectional drawings of the 2-, 3-, 4-kink soliton solutions of Eq. (1.1) along the x-axis at different times with parameters: **a** $N = 2$, $p_1 = -2$, $p_2 = -3$, $q_1 = \frac{1}{4}$, $q_2 = \frac{3}{2}$, $k_1 = k_2 = 1$, $\eta_1^0 = \eta_2^0 = 0$; **b** $N = 3$, $p_1 = p_2 = p_3 = -1$, $q_1 = -\frac{1}{2}$, $q_2 = 1$, $q_3 = -\frac{1}{9}$, $k_1 = k_2 = k_3 = 2$, $\eta_1^0 = \eta_2^0 = \eta_3^0 = 0$; **c** $N = 4$, $p_1 = p_2 = p_3 = p_4 = -1$, $q_1 = -\frac{1}{2}$, $q_2 = 1$, $q_3 = -\frac{1}{9}$, $q_4 = -2$, $k_1 = k_2 = k_3 = k_4 = 2$, $\eta_1^0 = \eta_2^0 = \eta_3^0 = \eta_4^0 = 0$. (Color online)

not change. And the interactions between these kink-shaped solitons make the amplitudes at their intersections appear a transient anomaly (see Figs. 1, 2 and 3).

3 The breather solutions and the hybrid solutions of the (3+1)-dimensional gsww equation

The shapes of the breather solutions undergo periodic oscillations during the propagation of the (3+1)-dimensional generalized shallow water wave. Their essence is in intimate relationship with multi-soliton solutions, which are generated based on the exponential function. Therefore, the hybrid solutions composed of multi-soliton solutions and breather solutions can also be discussed intensively in this section. Following the previous research [60–63], the N-soliton solution can be derived into the mth-order breather solution by first restricting the parameters in formula (2.21), (2.22) with the complex conjugate constraint

$$N = 2m, \quad p_{2i} = p_{2i-1}^*,$$
$$q_{2i} = q_{2i-1}^*, \quad k_{2i} = k_{2i-1}^*, \tag{3.1}$$

where $m \in N_+$, $i = 1, 2, \cdots, m$, and then continuing to select specific values for assignment. For instance, by setting the parameters $N = 2$, $p_2 = p_1^* = 2i$, $q_2 = q_1^* = 1 + 2i$, $k_2 = k_1^* = -3i$, $\eta_1^0 = \eta_2^0 = 0$, the first-order breather solution of Eq. (1.1) can be constructed

as

$$u_{1b} = \frac{8e^{\zeta_1}\sin(\xi_1)}{1 + e^{\xi_2} + e^{\xi_2^*} + 41e^{\zeta_2}}, \tag{3.2}$$

where

$$\zeta_1 = -\frac{6}{5}t + y,$$
$$\zeta_2 = -\frac{12}{5}t + 2y,$$
$$\xi_1 = \frac{52}{5}t + 2x + 2y - 3z,$$
$$\xi_2 = \left(-\frac{6}{5} + \frac{52}{5}i\right)t + 2ix + (1 + 2i)y - 3iz. \tag{3.3}$$

Thus it can be seen, the travel trajectory of the first-order breather solution u_{1b} along the x-axis is periodic, and the cycle period is π (see Fig. 4a, b and c). u_{1b} exhibits localization simultaneously in the y-direction on the (x, y)-plane. Besides that, while taking $N = 2$, $p_2 = p_1^* = q_1 = q_2^* = k_2 = k_1^* = 1 - i$, $\eta_1^0 = \eta_2^0 = 0$, the first-order kink-shaped breather solution of Eq. (1.1) is also shown in Fig. 4d, e and f. This breather solution not only exhibits kink feature in shape, but also exhibits oblique breathing behavior in the (x, y)-plane, with periodicity in both x and y directions.

When higher order cases are considered, by setting the parameters $N = 4$, $p_2 = p_1^* = k_2 = k_1^* = -i$, $q_2 = q_1^* = 1 + i$, $\eta_1^0 = \eta_2^0 = 2\pi$, $p_4 = p_3^* = k_4 = k_3^* = 2i$, $q_4 = q_3^* = 2 - 2i$, $\eta_3^0 = \eta_4^0 = -2\pi$ in formula

(a) $t = 0$ (b) $t = 0$ (c) $t = 0$

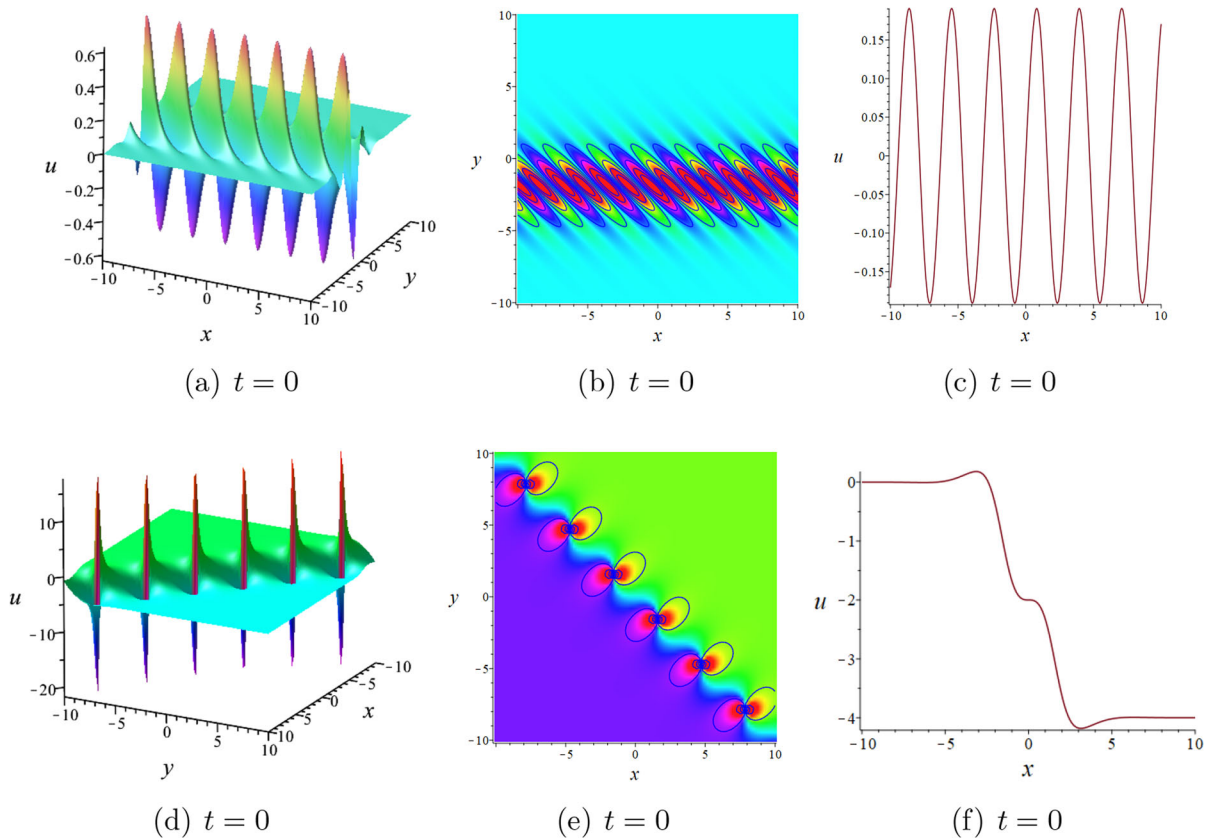(d) $t = 0$ (e) $t = 0$ (f) $t = 0$

Fig. 4 The first-order breather solution and the first-order kink-shaped breather solution of Eq. (1.1) in the (x, y)-plane at $t = 0$. **a, d** The 3D plot. **b, e** The density plot with contours. **c, f** The sectional drawing($y = 0$, $z = 0$). (Color online)

(2.21), (2.22), the second-order breather solution of Eq. (1.1) can be pushed out. The diagram shows that two rows of breather waves are spread in parallel (see Fig. 5a and b). Similar to the first-order breather solution at $N = 2$, the periodicity of the second-order breather solution is manifested in the x-direction on the (x, y)-plane, and the locality is manifested in the y-direction.

And the second-order kink-shaped breather solution of Eq. (1.1) can also be sought in like wise by taking $N = 4$, $p_2 = p_1^* = q_1 = q_2^* = k_2 = k_1^* = 1 - i$, $\eta_1^0 = \eta_2^0 = 2\pi$, $p_4 = p_3^* = q_3 = q_4^* = 2 + 2i$, $k_4 = k_3^* = -2 + 2i$, $\eta_3^0 = \eta_4^0 = -2\pi$ in formula (2.21), (2.22) (see Fig. 5c and d). The second-order kink-shaped breather solution exhibits periodic-

ity in both x and y directions, and its two kink-shaped breather waves propagate diagonally parallel to each other in the (x, y)-plane.

For $N > 3$, the two groups of parameters are restricted to be conjugate, and the remaining parameters are all real numbers in formula (2.21), (2.22), then the hybrid solutions consisting of the soliton solutions and the breather solutions of Eq. (1.1) can be derived. While taking $N = 3$, $p_1 = -q_1 = k_1 = 1$, $p_3 = p_2^* = k_3 = k_2^* = i$, $q_3 = q_2^* = -1 - i$, $\eta_1^0 = \eta_2^0 = \eta_3^0 = 0$, the hybrid solution of the first-order breather solution and the 1-kink soliton solution is given as follows

Fig. 5 The second-order breather solution and the second-order kink-shaped breather solution of Eq. (1.1) in the (x, y)-plane at $t = 0$. **a, c** The 3D plot. **b, d** The density plot with contours. (Color online)

(a) $t = 0$

(b) $t = 0$

(c) $t = 0$

(d) $t = 0$
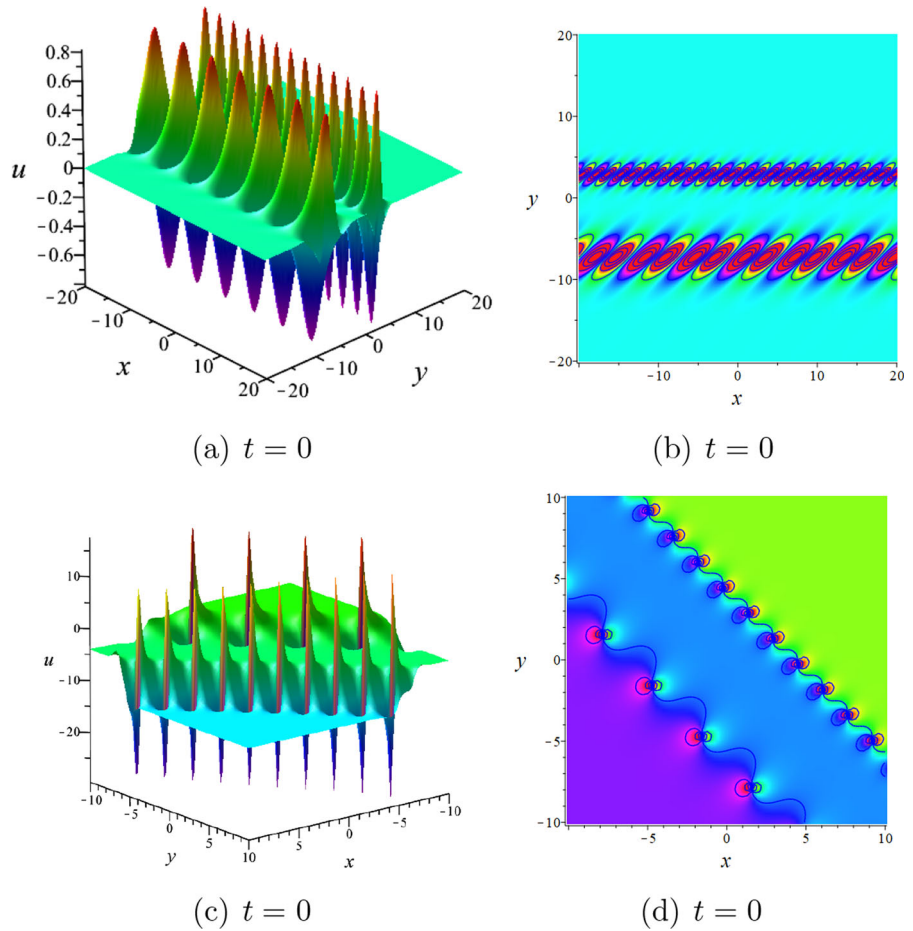
$$u_{1b-1s} = \frac{-(238 + 70i)e^{\delta_1} + (-238 + 70i)e^{\delta_1^*} + 314i(e^{\delta_2} - e^{\delta_2^*}) + 314e^{\nu_1} + 686e^{\nu_2}}{(77 - 42i)e^{\delta_1} + (77 + 42i)e^{\delta_1^*} - 157(e^{\delta_2} + e^{\delta_2^*} + e^{\nu_1}) - 343e^{\nu_2} - 1099e^{-t-2y} - 157},$$ (3.4)

where

$$\delta_1 = \left(-\frac{1}{2} + \frac{3}{2}i\right)t + (1 + i)x - (2 + i)y + (1 + i)z,$$

$$\delta_2 = \left(-\frac{1}{2} + \frac{3}{2}i\right)t + ix - (1 + i)y + iz,$$

$$\nu_1 = x - y + z,$$

$$\nu_2 = -t + x - 3y + z.$$ (3.5)

The collision effect between two different types of solutions does not destroy the periodicity of the first-order breather solution of Eq. (1.1) (see Fig. 6a and b).

Interestingly, when the parameters in formula (2.21), (2.22) are adjusted to the same values as above, the hybrid solution u_{1b-1s} appears as the interaction solu-

tion of the first-order periodic line wave and the 1-kink soliton in the (x, z)-plane. In the dynamic behavior of this hybrid solution of Eq. (1.1), the periodic line wave, also known as the line breather, appears from a constant background wave within a finite time interval in the middle and generates the maximum amplitude at $t = 0$, but it will eventually degenerate into the same constant background wave as time goes on (see Fig. 7). This first-order periodic line wave is a homoclinic orbital wave with uniformly varying wave heights in the (x, z)-plane. A key visual difference between it and the first-order breather solution of Eq. (1.1) is that the former

Fig. 6 The hybrid solutions of the first-order breather solution and the 1-kink soliton solution, the first-order kink-shaped breather solution and the 1-kink soliton solution of Eq. (1.1) in the (x, y)-plane at $t = 0$. **a**, **c** The 3D plot. **b**, **d** The density plot with contours. (Color online)

(a) $t = 0$

(b) $t = 0$

(c) $t = 0$

(d) $t = 0$
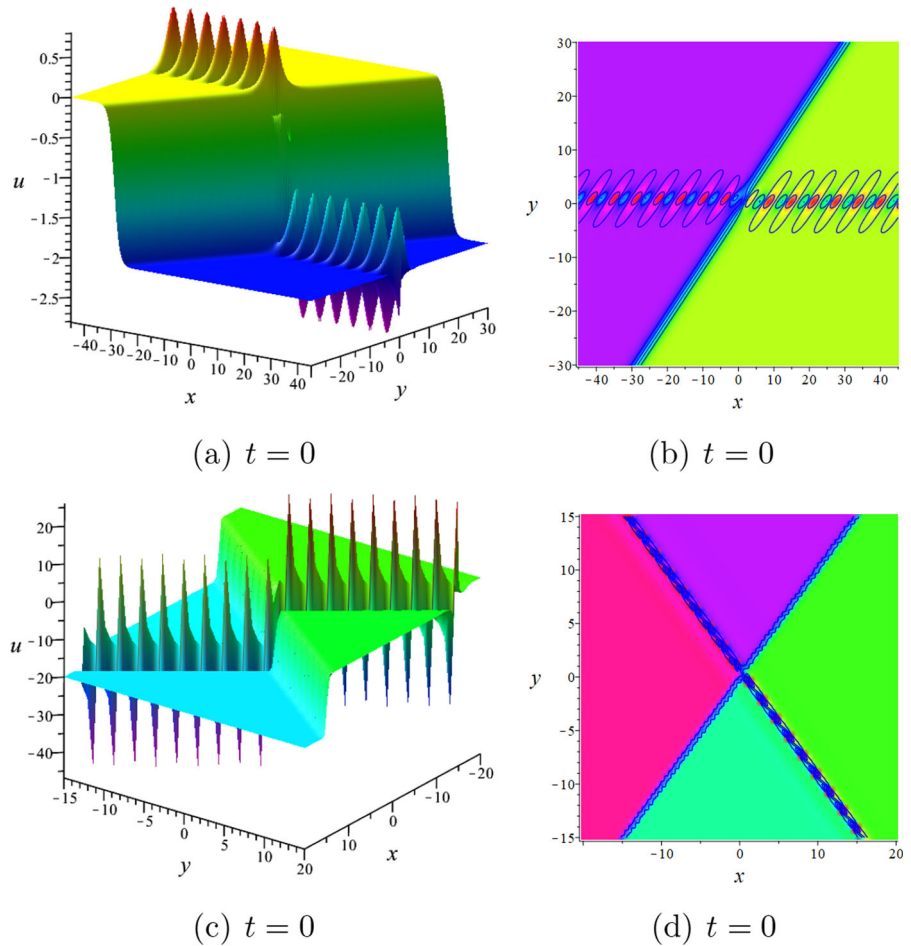
has periodicity in space and localization in time, while the periodicity and locality of the latter are respectively reflected in the x and y directions on the (x, y)-plane. This also means that the first-order line breather solution only exists for a limited short period of time. That is, when $|t| \gg 0$, the first-order periodic line wave will be almost completely immersed in the 1-kink soliton wave and only the 1-kink soliton will appear in the diagram of this hybrid solution.

Similarly, the mixed solution consisting of the first-order kink-shaped breather solution and the 1-kink soliton solution of Eq. (1.1) is also obtained under the parameters $N = 3$, $p_1 = -q_1 = k_1 = 8$, $p_3 = p_2^* = q_3 = q_2^* = k_2 = k_3^* = 1 + i$, $\eta_1^0 = \eta_2^0 = \eta_3^0 = 0$ (see Fig. 6c and d). These hybrid solutions are all definitely derived from the expansion of the 3-soliton solution of Eq. (1.1).

By taking $N = 4$, $p_2 = p_1^* = k_1 = k_2^* = i$, $q_2 = q_1^* = 1 + i$, $p_3 = p_4 = q_3 = -q_4 = -k_3 =$

$-k_4 = -1$, $\eta_1^0 = \eta_2^0 = \eta_3^0 = \eta_4^0 = 0$ in formula (2.21), (2.22), the hybrid solution of the first-order breather solution and the 2-kink soliton solution of Eq. (1.1) is shown in Fig. 8a, b and c.

The dynamic behavior of the hybrid solution consisting of the first-order kink-shaped breather solution and the 2-kink soliton solution can also be intuitively analyzed under the parameters $N = 4$, $p_2 = p_1^* = \frac{1}{6} + i$, $q_2 = q_1^* = \frac{5}{2} - i$, $k_2 = k_1^* = -\frac{1}{6} - i$, $p_3 = p_4 = q_3 = -q_4 = -k_3 = -k_4 = -1$, $\eta_1^0 = \eta_2^0 = \eta_3^0 = \eta_4^0 = 0$ in Fig. 8d, e and f. These hybrid solutions are solved based on the 4-soliton solution of Eq. (1.1). One thing that can be obviously observed is that in the dynamic behavior of these hybrid solutions, the collision between the 2-kink soliton solutions and the breather solutions of Eq. (1.1) does not disrupt the periodicity in the x-direction and the localization in the y-direction of the breathers on the (x, y)-plane, and the breathers maintain their original oscillating waveforms for propagation.

(a) $t = -15$

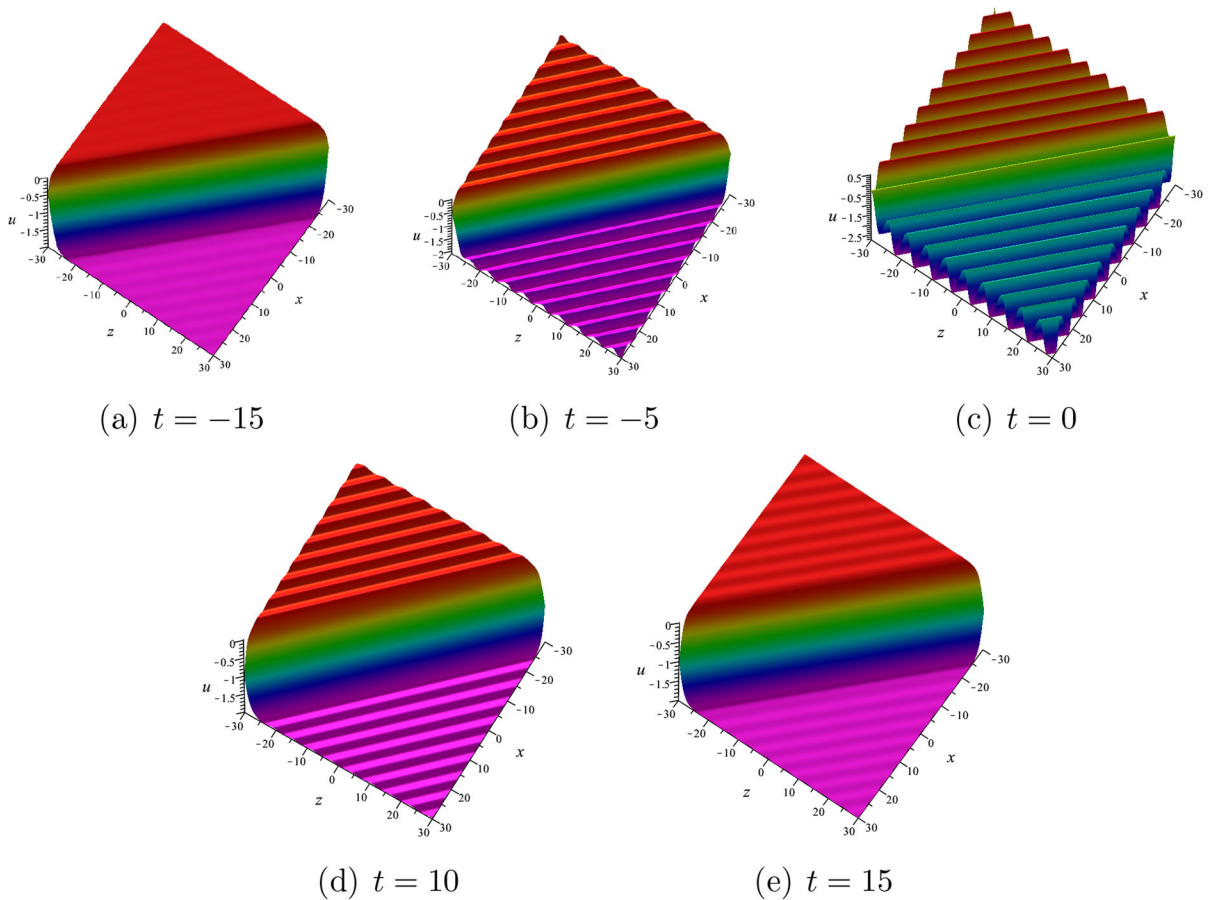(b) $t = -5$

(c) $t = 0$

(d) $t = 10$

(e) $t = 15$

Fig. 7 The hybrid solution of the first-order periodic solution and the 1-kink soliton solution of Eq. (1.1) in the (x, z)-plane at different times with parameters: $N = 3$, $p_1 = -q_1 = k_1 = 1$, $p_3 = p_2^* = k_3 = k_2^* = i$, $q_3 = q_2^* = -1-i$, $\eta_1^0 = \eta_2^0 = \eta_3^0 = 0$. **a** $t = -15$. **b** $t = -5$. **c** $t = 0$. **d** $t = 10$. **e** $t = 15$. (Color online)

4 The rational solutions of the (3+1)-dimensional gsww equation

In view of the earlier research [59–63], the rational solutions of nonlinear waves can be derived by taking the long wave limits of the soliton solutions based on the Hirota bilinear method. The lump solutions of the (3+1)-dimensional generalized shallow water wave equation, as some special rational function solutions localized in space, will be discussed emphatically in this section.

Case I

Consider the case of $N = 2$.

The parameters in formula (2.21), (2.22) are stipulated as follows

$$N = 2, \quad q_1 = \lambda_1 p_1, \quad k_1 = \gamma_1 p_1, \quad q_2 = \lambda_2 p_2,$$
$$k_2 = \gamma_2 p_2, \quad \eta_1^0 = \eta_2^0 = i\pi, \tag{4.1}$$

and then the limits $p_i \to 0$ $(i = 1, 2)$ are performed. Hence, the f in formula (2.21) is rewritten as a polynomial function

$$f = \theta_1 \theta_2 + \alpha_{12}, \tag{4.2}$$

(a) $t = -10$

(b) $t = 0$

(c) $t = 10$

(d) $t = -10$
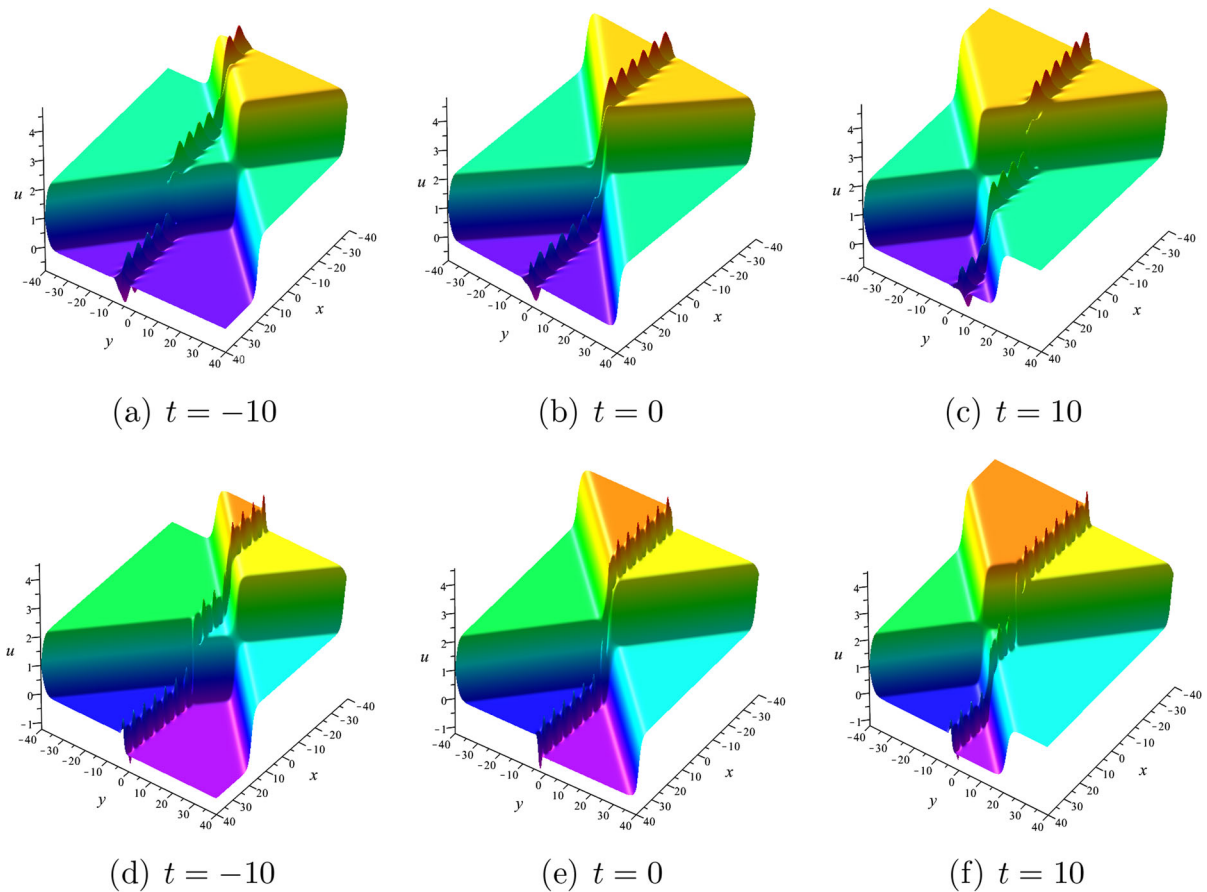
(e) $t = 0$

(f) $t = 10$

Fig. 8 The hybrid solutions of the first-order breather solution and the 2-kink soliton solution, the first-order kink-shaped breather solution and the 2-kink soliton solution of Eq. (1.1) in the (x, y)-plane at different times. **a, d** $t = -10$. **b, e** $t = 0$. **c, f** $t = 10$. (Color online)

where

$$\theta_i = \frac{y\lambda_i^2 + (z\gamma_i + x)\lambda_i - t\gamma_i}{\lambda_i}, \quad (i = 1, 2),$$

$$\alpha_{12} = -\frac{6\lambda_1\lambda_2(\lambda_1 + \lambda_2)}{(\lambda_1 - \lambda_2)(\gamma_1\lambda_2 - \gamma_2\lambda_1)}. \tag{4.3}$$

Letting $\lambda_2 = \lambda_1^* = -i$, $\gamma_1 = \gamma_2 = 1$, and combining the transformation (2.3), the first-order lump solution of Eq. (1.1) is solved as

$$u_{1-lump} = \frac{-4(x + z)}{(x + z)^2 + (t + y)^2}. \tag{4.4}$$

The dynamic behavior of the first-order lump solution u_{1-lump} at different times is shown in Fig. 9.

Due to the concentrated distribution of energy, it produces a local lump with two wave crests, one above the horizontal plane and the other below the horizontal

plane, resulting in this lump presenting a wave peak and a wave trough. It can be intuitively found that in a finite space, u_{1-lump}, as a rational solution of Eq. (1.1), maintains a perfect profile around the control center of its waveform and moves on a constant background without diffusion or collapse. Nevertheless when $x \to \pm\infty$ or $y \to \pm\infty$, the first-order lump solution u_{1-lump} degenerates to 0, which indicates that its asymptotic background is zero.

It is worth mentioning that when the parameters in formula (2.21), (2.22) is constrained to $p_2 = p_1^* = q_2 = q_1^* = k_1 = k_2^* = 1 + i$, $\eta_1^0 = \eta_2^0 = 0$, the first-order breather solution is transformed into the first-order line rogue wave (RW) solution of Eq. (1.1) as follows

Fig. 9 The first-order lump solution of Eq. (1.1) in the (x, y)-plane at different times. **a** $t = -30$. **b** $t = 0$. **c** $t = 30$. **d** The density plot with contours. (Color online)

(a) $t = -30$

(b) $t = 0$

(c) $t = 30$

(d) $t = 0$
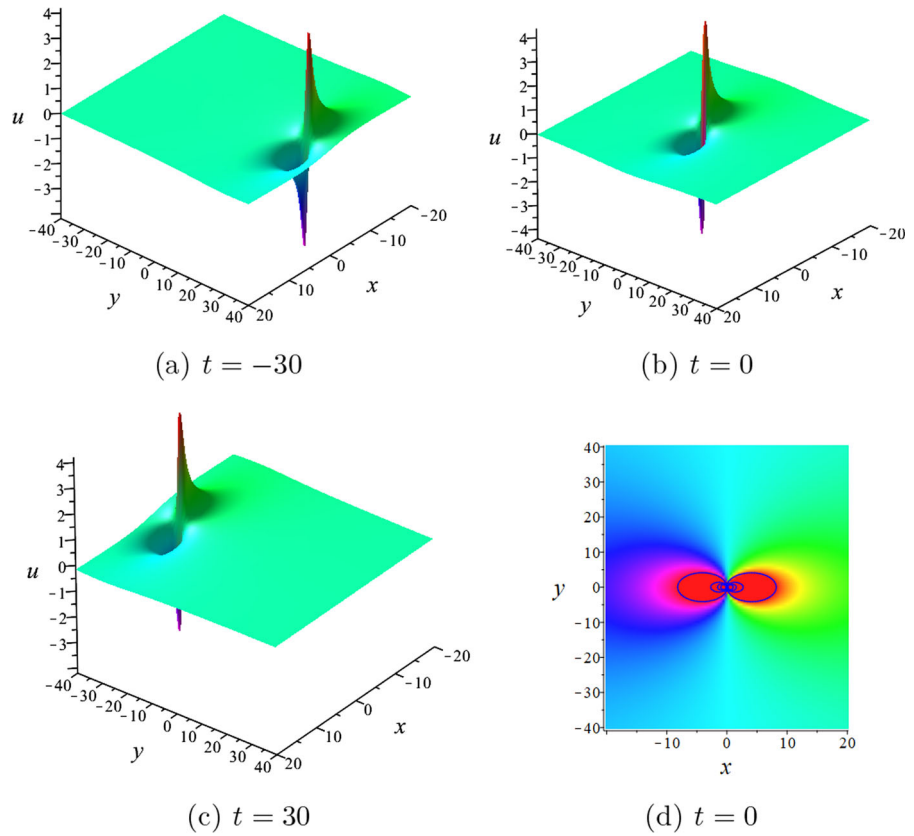
$$u_{RW} = \frac{(2+2i)e^{\chi_1} + (2-2i)e^{\chi_1^*} - 4e^{\chi_2}}{-1 - (e^{\chi_1} + e^{\chi_1^*}) + e^{\chi_2}}, \qquad (4.5)$$

where

$$\chi_1 = (1-i)t + (1+i)x + (1+i)y + (1-i)z, \\ \chi_2 = 2t + 2x + 2y + 2z. \qquad (4.6)$$

The first-order line rogue wave, as a finite form of the first-order line breather solution of Eq. (1.1), is generated in a constant background, rising or decaying with time evolution, and its maximum wave crest value appears at $t = 0$ and $x + y = 0$ (see Fig. 10). The first-order line rogue wave solution of Eq. (1.1) is localized in time and space, and the wave height at infinity of the (x, y)-plane tends to zero. Therefore, this line wave has the typical characteristic of a rogue wave solution: coming and going without a trace.

Case II

Consider the case of N=4.

By constraining the parameters in formula (2.21), (2.22) as

$$N = 4, \quad q_1 = \lambda_1 p_1, \quad k_1 = \gamma_1 p_1,$$
$$q_2 = \lambda_2 p_2, \quad k_2 = \gamma_2 p_2,$$
$$q_3 = \lambda_3 p_3, \quad k_3 = \gamma_3 p_3, \quad q_4 = \lambda_4 p_4, \quad k_4 = \gamma_4 p_4,$$
$$\eta_1^0 = \eta_2^0 = \eta_3^0 = \eta_4^0 = i\pi, \qquad (4.7)$$

and performing the limits $p_i \to 0$ ($i = 1, 2, 3, 4$), the f in formula (2.21) is completely transformed from a exponential function to a purely rational function as follows

$$f = \theta_1\theta_2\theta_3\theta_4 + \alpha_{12}\theta_3\theta_4 + \alpha_{13}\theta_2\theta_4 + \alpha_{14}\theta_2\theta_3$$
$$+ \alpha_{23}\theta_1\theta_4 + \alpha_{24}\theta_1\theta_3 + \alpha_{34}\theta_1\theta_2$$
$$+ \alpha_{12}\alpha_{34} + \alpha_{13}\alpha_{24} + \alpha_{14}\alpha_{23},$$

$$(4.8)$$

where

$$\theta_i = \frac{y\lambda_i^2 + (z\gamma_i + x)\lambda_i - t\gamma_i}{\lambda_i},$$
$$\alpha_{ij} = -\frac{6\lambda_i\lambda_j(\lambda_i + \lambda_j)}{(\lambda_i - \lambda_j)(\gamma_i\lambda_j - \gamma_j\lambda_i)},$$
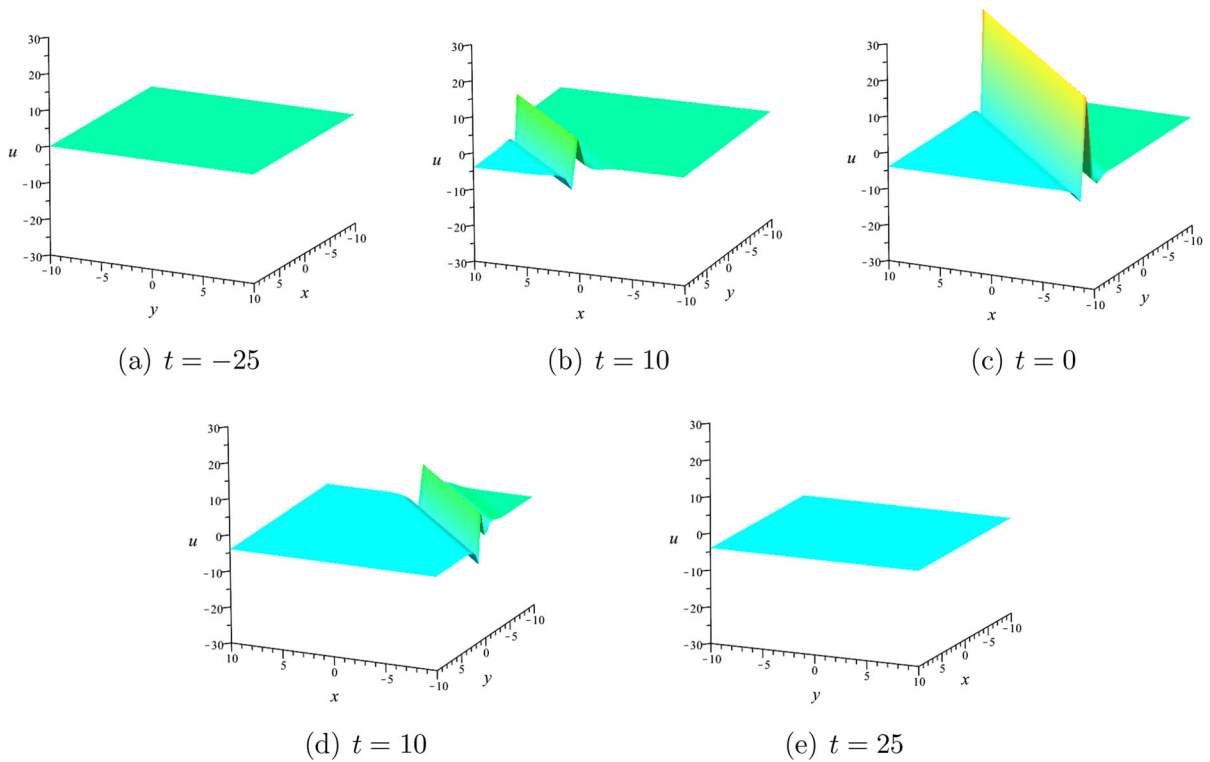
Fig. 10 The first-order line rogue wave solution of Eq. (1.1) in the (x, y)-plane at different times. **a** $t = -25$. **b** $t = 10$. **c** $t = 0$. **d** $t = 10$. **e** $t = 25$. (Color online)

$$(i < j, i, j = 1, 2, 3, 4). \tag{4.9}$$

Taking $\lambda_2 = \lambda_1^* = -i$, $\lambda_4 = \lambda_3^* = -2i$, $\gamma_1 = \gamma_2 = \gamma_3 = \gamma_4 = 1$, and combining the transformation (2.3), the second-order lump solution of Eq. (1.1) is presented as

$$
\begin{aligned}
u_{2-lump} &= (-288x^3 - 864x^2z - (36\rho_1 + 864z^2)x \\
&\quad -288z^3 - 36\rho_1 z - 7872t - 15360y)/(36x^4 + 144x^3z \\
&\quad +(9\rho_1 + 216z^2)x^2 + (144z^3 + 18\rho_1 z + 3936t \\
&\quad +7680y)x + 36z^4 + 9\rho_1 z^2 + (3936t + 7680y)z \\
&\quad +9\rho_2 t^2 + 360ty^3 + 144y^4 + 46720),
\end{aligned} \tag{4.10}
$$

where

$$
\begin{aligned}
\rho_1 &= 5t^2 + 16ty + 20y^2, \\
\rho_2 &= t^2 + 10ty + 33y^2.
\end{aligned} \tag{4.11}
$$

The intuitive diagram of the second-order lump solution u_{2-lump} is also given (see Fig. 11).

After the evolution of t, u_{2-lump} only undergoes parallel shift in asymptotic motion, but its permanent lumps pattern does not change. Thus, the form of

u_{2-lump} at $t = 0$ is discussed without losing generality. The wave crests and troughs of u_{2-lump} have doubled compared to the first-order lump solution of Eq. (1.1). Additionally, when $x \to \pm\infty$ or $y \to \pm\infty$, the second-order lump solution u_{2-lump} will also degenerate to zero and disappear from the field of view.

5 The semi-rational solutions of the (3+1)-dimensional gsww equation

The key to the construction of the semi-rational solutions of Eq. (1.1) lies in the application of taking the long wave limit of partial exponential functions similar to Sect. 4 and the special restrictions on the parameters in formula (2.21), (2.22).

When $N = 3$, by setting the parameters in formula (2.21), (2.22) as

$$
\begin{aligned}
&N = 3, \quad q_1 = \lambda_1 p_1, \quad k_1 = \gamma_1 p_1, \quad q_2 = \lambda_2 p_2, \\
&k_2 = \gamma_2 p_2, \quad \eta_1^0 = \eta_2^0 = i\pi,
\end{aligned} \tag{5.1}
$$

and taking the limits $p_1, p_2 \to 0$, the f in formula (2.21) can be updated as a combination of polynomial

Fig. 11 The second-order lump solution of Eq. (1.1) in the (x, y)-plane at $t = 0$. **a** The 3D plot. **b** The density plot with contours. (Color online)

(a) $t = 0$

(b) $t = 0$
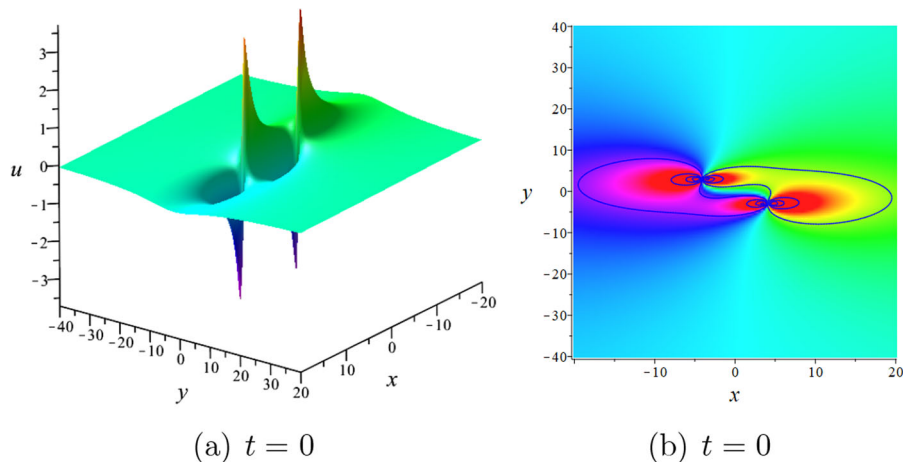
and exponential functions

$$f = (\theta_1\theta_2 + \alpha_{13}\theta_2 + \alpha_{23}\theta_1 + \alpha_{13}\alpha_{23} + \alpha_{12})e^{\eta_3}$$
$$+ \theta_1\theta_2 + \alpha_{12},$$
(5.2)

where

$$\alpha_{i3} = -\frac{6(p_3^2 q_3 \lambda_i^2 + p_3 q_3^2 \lambda_i)}{-p_3 k_3 \lambda_i^2 + (3p_3^2 q_3 + k_3 + p_3 \gamma_i)q_3\lambda_i - q_3^2\gamma_i},$$
$$(i = 1, 2),$$
(5.3)

and η_3 is the same as in (2.22), θ_i $(i = 1, 2)$, α_{12} are the same as in (4.3). In particular, if the parameters $\lambda_2 = \lambda_1^* = -2i$ and the remaining parameters are all real numbers, such as $\gamma_1 = \gamma_2 = 1$, $p_3 = q_3 = k_3 = -2$, $\eta_3^0 = 0$, and then combining the transformation (2.3), the semi-rational solution of Eq. (1.1) consisting of the first-order lump solution and the 1-kink soliton solution can be obtained as

$$u_{lump-1s} = ((12688(x^2 + z^2) + (25376z + 4208)x$$
$$+ 4208z + 3172t^2 + (25376y + 22656)t$$
$$+ 50752y^2 + 90624y + 37632)e^{\tau}$$
$$- 12688(x + z))/((3172(x^2 + z^2) + (6344z$$
$$+ 4224)x + 4224z + 793t^2 + (6344y + 5664)t$$
$$+ 12688y^2 + 22656y + 11520)e^{\tau}$$
$$+ 3172x^2 + 6344xz + 3172z^2 + 793(t + 4y)^2),$$
(5.4)

where

$$\tau = 10t - 2x - 2y - 2z.$$
(5.5)

The first-order lump will pass through the 1-kink soliton of Eq. (1.1) over time. Their collision is elastic, and the amplitude increases and the energy is concentrated at the intersection (see Fig. 12).

By the same means, the dynamic behavior of the semi-rational solution of Eq. (1.1) consisting of the first-order line rogue wave and the 1-kink soliton is further presented. It can be seen intuitively that the collision between the first-order line rogue wave and the 1-kink soliton results in the maximum amplitude at $t = 0$ and $x + z = 0$ (see Fig. 13). In addition, because the line rogue wave is localized in space and time, it will degenerate into a constant plane wave when $|t| \gg 0$, that is, only the 1-kink soliton can be seen at this time, and the amplitude of the line rogue wave of Eq. (1.1) tends to zero at the infinity of the (x, z)-plane.

When $N = 4$, the parameters are constrained in formula (2.21), (2.22) as follows

$$N = 4, \quad q_1 = \lambda_1 p_1, \quad k_1 = \gamma_1 p_1, \quad q_2 = \lambda_2 p_2,$$
$$k_2 = \gamma_2 p_2, \quad \eta_1^0 = \eta_2^0 = i\pi,$$
(5.6)

and then the limits $p_1, p_2 \to 0$ are performed. Thus, the f in formula (2.21) is rewritten as

$$f = (\theta_1\theta_2 + \alpha_{13}\theta_2 + \alpha_{23}\theta_1 + \alpha_{13}\alpha_{23} + \alpha_{12})e^{\eta_3}$$
$$+ (\theta_1\theta_2 + \alpha_{14}\theta_2 + \alpha_{24}\theta_1 + \alpha_{14}\alpha_{24} + \alpha_{12})e^{\eta_4}$$
$$+ (\theta_1\theta_2 + \alpha_{13}\theta_2 + \alpha_{14}\theta_2 + \alpha_{23}\theta_1 + \alpha_{24}\theta_1$$
$$+ \alpha_{13}\alpha_{23} + \alpha_{13}\alpha_{24} + \alpha_{14}\alpha_{23} + \alpha_{14}\alpha_{24}$$
$$+ \alpha_{12})e^{\eta_3+\eta_4+A_{34}} + \theta_1\theta_2 + \alpha_{12},$$
(5.7)

where

$$\alpha_{i4} =$$
$$-\frac{6(p_4^2 q_4 \lambda_i^2 + p_4 q_4^2 \lambda_i)}{-p_4 k_4 \lambda_i^2 + (3p_4^2 q_4 + k_4 + p_4 \gamma_i)q_4\lambda_i - q_4^2\gamma_i},$$

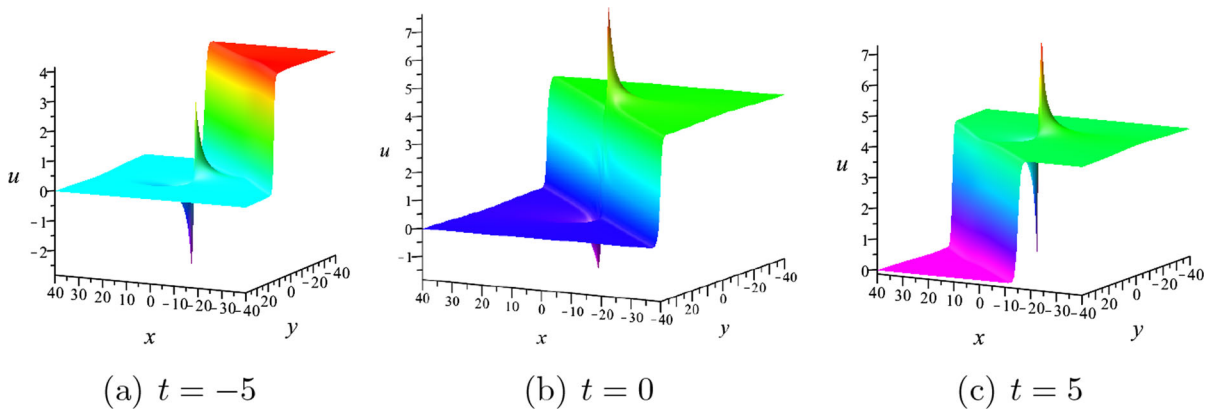(a) $t = -5$ (b) $t = 0$ (c) $t = 5$

Fig. 12 The semi-rational solution consisting of the first-order lump solution and the 1-kink soliton solution of Eq. (1.1) in the (x, y)-plane at different times. **a** $t = -5$. **b** $t = 0$. **c** $t = 5$. (Color online)
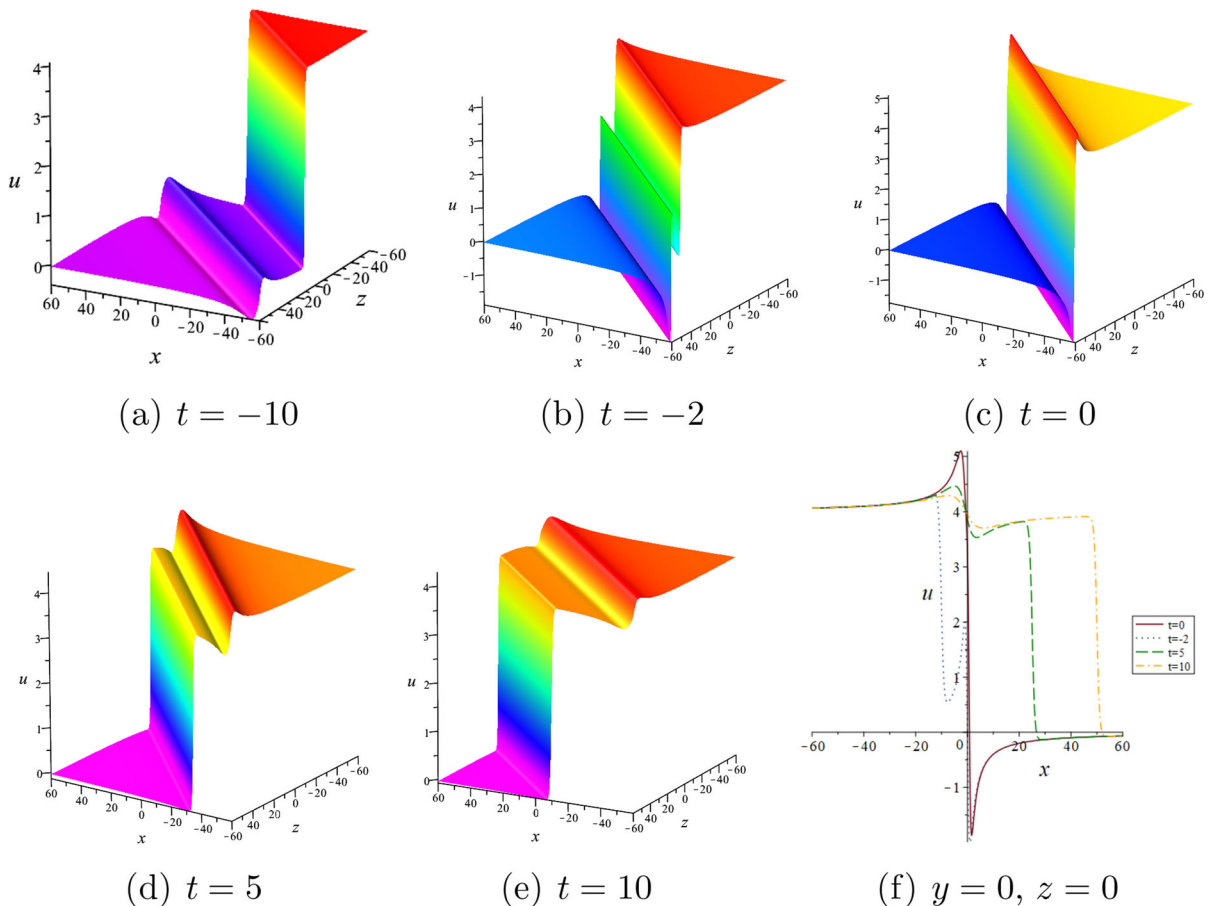

(a) $t = -10$ (b) $t = -2$ (c) $t = 0$

(d) $t = 5$ (e) $t = 10$ (f) $y = 0, z = 0$

Fig. 13 The semi-rational solution consisting of the first-order line rogue wave solution and the 1-kink soliton solution of Eq. (1.1) in the (x, z)-plane at different times with parameters: $N = 3$, $\lambda_2 = \lambda_1^* = -2i$, $\gamma_1 = \gamma_2 = 1$, $p_3 = q_3 = k_3 = -2$, $\eta_3^0 = 0$. **a** $t = -10$. **b** $t = -2$. **c** $t = 0$. **d** $t = 5$. **e** $t = 10$. **f** The sectional drawing. (Color online)

(a) $t = 0$ (b) $t = 0$ (c) $t = 0$
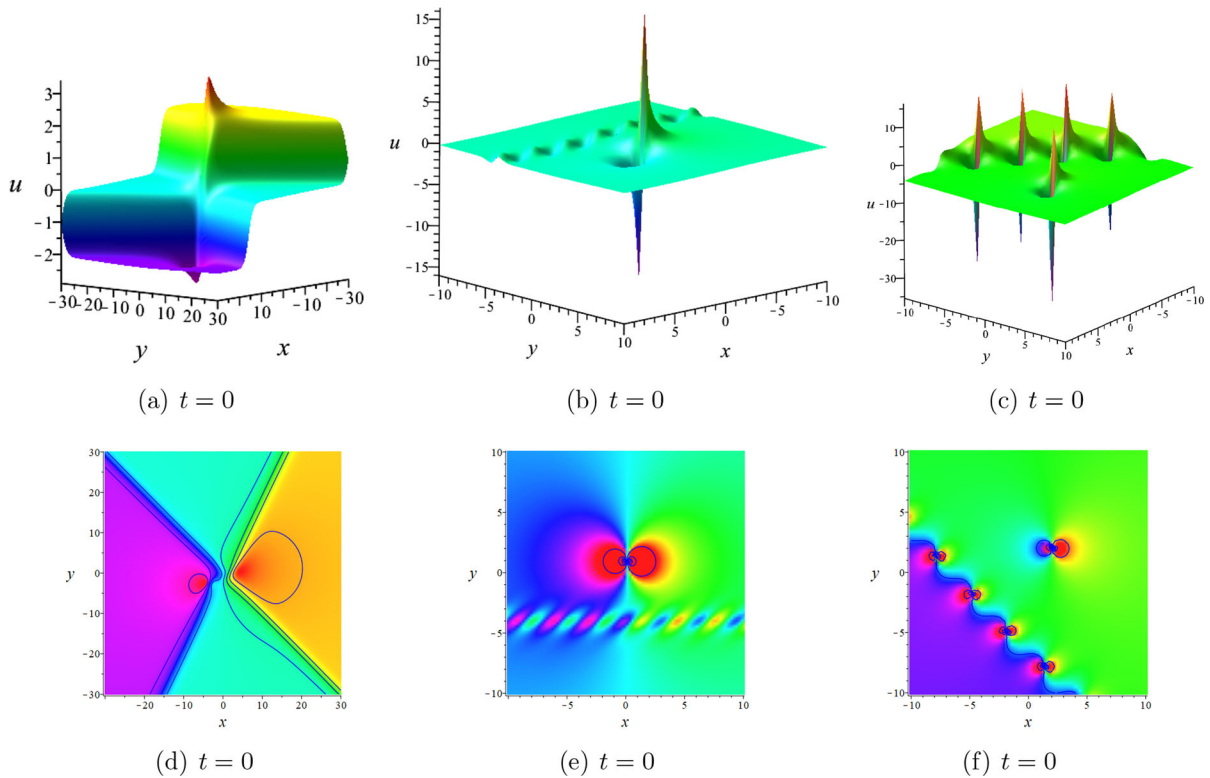
(d) $t = 0$ (e) $t = 0$ (f) $t = 0$

Fig. 14 The semi-rational solutions consisting of the first-order lump solution and the 2-kink soliton solution, the first-order lump solution and the first-order breather solution, the first-order lump solution and the first-order kink-shaped breather solution of Eq. (1.1) in the (x, y)-plane at $t = 0$. **a, b, c** The 3D plot. **d, e, f** The density plot with contours. (Color online)

$$(i = 1, 2), \tag{5.8}$$

and α_{i3} $(i = 1, 2)$ are the same as in (5.3), η_3, η_4, $e^{A_{34}}$ are the same as in (2.22), θ_i $(i = 1, 2)$, α_{12} are the same as in (4.3). Here, if the parameters $\lambda_2 = \lambda_1^* = -i$ and the remaining parameters are all real numbers as $\gamma_1 = \gamma_2 = p_3 = -p_4 = q_3 = 2q_4 = k_3 = -k_4 = 1$, $\eta_3^0 = \eta_4^0 = 0$, and then combining the transformation (2.3), the semi-rational solution of Eq. (1.1) consisting of the first-order lump solution and the 2-kink soliton solution can be proposed (see Fig. 14a and d).

However, when the parameters $\lambda_2 = \lambda_1^* = -i$, $\gamma_1 = \gamma_2 = 1$, and the remaining two groups of parameters are restricted to be complex conjugate, two kinds of the semi-rational solutions of Eq. (1.1) can be constructed. If the remaining parameters $p_4 = p_3^* = k_4 = k_3^* = 2i$, $q_4 = q_3^* = 2 - 2i$, $\eta_3^0 = \eta_4^0 = 2\pi$, the semi-rational solution consisting of the first-order lump solution and the first-order breather solution can be derived (see Fig. 14b and e). When the remaining parameters

$p_4 = p_3^* = q_3 = q_4^* = 1 + i$, $k_4 = k_3^* = 1 - 2i$, $\eta_3^0 = \eta_4^0 = 2\pi$, the semi-rational solutions consisting of the first-order lump solution and the first-order kink-shaped breather solution is presented (see Fig. 14c and f). For these lump-soliton and lump-breather semi-rational solutions, when $\eta_i^0 \to 0$ $(i = 3, 4)$, the lump will collide with the 2-kink soliton of Eq. (1.1) (see Fig. 14a and d). When $|\eta_i^0| \gg 0$ $(i = 3, 4)$, the lump will completely separate from the breathers of Eq. (1.1), and the periodicity and amplitude of the breather solutions remain stable (see Fig. 14b and e, c and f).

6 Conclusions

Some exact solutions of the (3+1)-dimensional generalized shallow water wave equation and the dynamic behaviors between them are systematically studied in this paper. The explicit N-soliton solution of Eq. (1.1) is derived based on the Hirota bilinear method and

the standard perturbation method. The multi-soliton solutions of Eq. (1.1) exhibit kink characteristics due to $p_i \neq 0$ ($i = 1, 2, \cdots, N$), and the elastic collision behaviors of these solutions are discussed (see Figs. 1, 2 and 3). By adding constraints to the parameters of the original N-soliton solution, the higher-order breather solutions of Eq. (1.1) with periodic oscillation and localization on the (x, y)-plane are also solved (see Figs. 4 and 5). The hybrid solutions consisting of two types of breather solutions, the kink-shaped soliton solutions and the periodic solution (see Figs. 6, 7 and 8), and the line rogue wave solution (see Fig. 10) together enrich the dynamic behaviors between different types of solutions of Eq. (1.1). It can be seen that both the periodic solution and the line rogue wave solution grow and decay over time in a constant background.

In addition, the lump solutions (see Fig. 9, 11) are constructed by taking the long wave limit of the soliton solutions of Eq. (1.1). The difference between the line rogue wave solution and the lump solution is not only reflected in their shapes, but also in their localities, that is, the former has locality in both time and space, while the latter only has locality in space. When $N > 2$, the dynamic behaviors of Eq. (1.1) are better described by the semi-rational solutions consisting of the lump, the kink-shaped solitons, the line rogue wave and the breathers (see Figs. 12, 13 and 14). Some special constraints of the parameters play an important role in affecting the diversity and the dynamic behaviors of these solutions. It's worth noting that the higher-order kink-shaped soliton and breather solutions, the line rogue wave solution, the RW-soliton and lump-breather semi-rational solutions, and the hybrid solutions consisting of the breather solutions, the kink-shaped soliton solutions and the periodic solution of Eq. (1.1) have never been reported in the previous literature. The dynamic behaviors of these solutions constructed in this paper also reflect the amazing ordering caused by nonlinear actions. The research results of this paper are helpful to the research of other (3+1)-dimensional nonlinear evolution equations, enrich the theory of nonlinear dynamic systems, and help explain some nonlinear physical phenomena in nature.

Data availability The data that support the findings of this article are available from the corresponding author, upon reasonable request.

Declarations

Conflict of interest The authors declare that they have no conflict of interest.

Ethical approval The authors declare that they comply with ethical standards.

References

1. Gu, C., Guo, B., Li, Y., et al.: Soliton Theory and Its Applications. Springer, Berlin (1995)
2. Zabusky, N.J., Kruskal, M.D.: Interaction of "solitons" in a collisionless plasma and the recurrence of initial states. Phys. Rev. Lett. **15**, 240–243 (1965)
3. Gardner, C.S., Greene, J.M., Kruskal, M.D., Miura, R.M.: Method for solving the Korteweg-deVries equation. Phys. Rev. Lett. **19**, 1095–1097 (1967)
4. Zakharov, V.E., Shabat, A.B.: A scheme for integrating the nonlinear equations of mathematical physics by the method of the inverse scattering problem. I. Funktsional. Anal. i Prilozhen. **8**, 43–53 (1974)
5. Ablowitz, M.J., Clarkson, P.A.: Solitons, Nonlinear Evolution Equations and Inverse Scattering. Cambridge University Press, Cambridge (1991)
6. Wang, M., Zhou, Y., Li, Z.: Application of a homogeneous balance method to exact solutions of nonlinear equations in mathematical physics. Phys. Lett. A **216**, 67–75 (1996)
7. Fan, E.: Two new applications of the homogeneous balance method. Phys. Lett. A **265**, 353–357 (2000)
8. Fu, Z., Liu, S., Liu, S., et al.: Jacobi elliptic function expansion method and periodic wave solutions of nonlinear wave equations. Phys. Lett. A **289**, 69–74 (2001)
9. Zhang, H.: Extended Jacobi elliptic function expansion method and its applications. Commun. Nonlinear Sci. Numer. Simul. **12**, 627–635 (2007)
10. Ma, W.X., Abdeljabbar, A.: A bilinear Bäcklund transformation of a (3+1)-dimensional generalized KP equation. Appl. Math. Lett. **25**, 1500–1504 (2012)
11. Hietarinta, J., Joshi, N., Nijhoff, F.W.: Discrete Systems and Integrability. Cambridge University Press, Cambridge (2016)
12. Lan, Z.Z., Gao, Y.T., Yang, J.W., et al.: Solitons, Bäcklund transformation and Lax pair for a (2+1)-dimensional Broer-Kaup-Kupershmidt system in the shallow water of uniform depth. Commun. Nonlinear Sci. Numer. Simul. **44**, 360–372 (2017)
13. Matveev, V.B., Salle, M.A.: Darboux Transformations and Solitons. Springer, Berlin (1991)
14. Gu, C., Hu, H., Zhou, Z.: Darboux transformations in integrable systems: theory and their applications to geometry. Springer, Berlin (2005)

15. Geng, X., Lv, Y.: Darboux transformation for an integrable generalization of the nonlinear Schrödinger equation. Nonlinear Dyn. **69**, 1621–1630 (2012)

16. Hirota, R.: Exact solution of the Korteweg-de Vries equation for multiple collisions of solitons. Phys. Rev. Lett. **27**, 1192–1194 (1971)

17. Hietarinta, J.: Introduction to the Hirota Bilinear Method. In: Kosmann-Schwarzbach, Y., Grammaticos, B., Tamizhmani, K.M. (eds.) Integrability of Nonlinear Systems, pp. 95–103. Springer, Heidelberg (1997)

18. Hirota, R.: The Direct Method in Soliton Theory. Cambridge University Press, Cambridge (2004)

19. Wazwaz, A.M.: Multiple-soliton solutions for the KP equation by Hirota′s bilinear method and by the tanh-coth method. Appl. Math. Comput. **190**, 633–640 (2007)

20. Freeman, N.C., Nimmo, J.J.C.: Soliton solutions of the Korteweg-de Vries and the Kadomtsev–Petviashvili equations: the Wronskian technique. Phys. Lett. A **95**, 1–3 (1983)

21. Ablowitz, M.J., Yaacov, D.B., Fokas, A.S.: On the inverse scattering transform for the Kadomtsev–Petviashvili equation. Stud. Appl. Math. **69**, 135–143 (1983)

22. Ma, W.X.: Lump solutions to the Kadomtsev–Petviashvili equation. Phys. Lett. A **379**, 1975–1978 (2015)

23. Ohta, Y., Yang, J.: Rogue waves in the Davey–Stewartson I equation. Phys. Rev. E **86**, 036604 (2012)

24. Ohta, Y., Yang, J.: Dynamics of rogue waves in the Davey–Stewartson II equation. J. Phys. A: Math. Theor. **46**, 105202 (2013)

25. Bao, W., Tang, Q., Xu, Z.: Numerical methods and comparison for computing dark and bright solitons in the nonlinear Schrödinger equation. J. Comput. Phys. **235**, 423–445 (2013)

26. Ren, P., Rao, J.: Bright-dark solitons in the space-shifted nonlocal coupled nonlinear Schrödinger equation. Nonlinear Dyn. **108**, 2461–2470 (2022)

27. Yuan, Y.Q., Tian, B., Liu, L., et al.: Solitons for the (2+1)-dimensional Konopelchenko–Dubrovsky equations. J. Math. Anal. Appl. **460**, 476–486 (2018)

28. Darvishi, M.T., Najafi, M., Arbabi, S., et al.: Exact propagating multi-anti-kink soliton solutions of a (3+1)-dimensional B-type Kadomtsev–Petviashvili equation. Nonlinear Dyn. **83**, 1453–1462 (2016)

29. Ding, C.C., Gao, Y.T., Deng, G.F.: Breather and hybrid solutions for a generalized (3+1)-dimensional B-type Kadomtsev–Petviashvili equation for the water waves. Nonlinear Dyn. **97**, 2023–2040 (2019)

30. Tao, Y., He, J.: Multisolitons, breathers, and rogue waves for the Hirota equation generated by the Darboux transformation. Phys. Rev. E **85**, 026601 (2012)

31. Xu, S., He, J.: The rogue wave and breather solution of the Gerdjikov–Ivanov equation. J. Math. Phys. **53**, 063507 (2012)

32. He, J., Wang, L., Li, L., et al.: Few-cycle optical rogue waves: complex modified Korteweg-de Vries equation. Phys. Rev. E **89**, 062917 (2014)

33. Villarroel, J., Prada, J., Estévez, P.G.: Dynamics of lump solutions in a 2+1 NLS equation. Stud. Appl. Math. **122**, 395–410 (2009)

34. Ma, W.X., Zhou, Y.: Lump solutions to nonlinear partial differential equations via Hirota bilinear forms. J. Differ. Equ. **264**, 2633–2659 (2018)

35. Foroutan, M., Manafian, J., Ranjbaran, A.: Lump solution and its interaction to (3+1)-D potential-YTSF equation. Nonlinear Dyn. **92**, 2077–2092 (2018)

36. Peregrine, D.H.: Water waves, nonlinear Schrödinger equations and their solutions. J. Aust. Math. Soc. Ser. B. **25**, 16–43 (1983)

37. Akhmediev, N., Ankiewicz, A., Taki, M.: Waves that appear from nowhere and disappear without a trace. Phys. Lett. A **373**, 675–678 (2009)

38. Dysthe, K., Krogstad, H.E., Muller, P.: Oceanic rogue waves. Annu. Rev. Fluid Mech. **40**, 287–310 (2008)

39. Solli, D.R., Ropers, C., Koonath, P., et al.: Optical rogue waves. Nature **450**, 1054–1057 (2007)

40. Bludov, Y.V., Konotop, V.V., Akhmediev, N.: Matter rogue waves. Phys. Rev. A **80**, 033610 (2009)

41. Bludov, Y.V., Konotop, V.V., Akhmediev, N.: Vector rogue waves in binary mixtures of Bose–Einstein condensates. Eur. Phys. J. Spec. Top. **185**, 169–180 (2009)

42. El-Awady, E.I., Moslem, W.M.: On a plasma having nonextensive electrons and positrons: Rogue and solitary wave propagation. Phys. Plasmas **18**, 082306 (2011)

43. Stenflo, L., Marklund, M.: Rogue waves in the atmosphere. J. Plasma Phys. **76**, 293–295 (2010)

44. Geng, X.: Algebraic-geometrical solutions of some multidimensional nonlinear evolution equations. J. Phys. A: Math. Gen. **36**, 2289–2303 (2003)

45. Geng, X., Ma, Y.: *N*-soliton solution and its Wronskian form of a (3+1)-dimensional nonlinear evolution equation. Phys. Lett. A **369**, 285–289 (2007)

46. Öziş, T., Aslan, İ: Exact and explicit solutions to the (3+1)-dimensional Jimbo–Miwa equation via the Exp-function method. Phys. Lett. A **372**, 7011–7015 (2008)

47. Ma, W.X.: Lump-type solutions to the (3+1)-dimensional Jimbo–Miwa equation. Int. J. Nonlinear Sci. Numer. Simul. **17**, 355–359 (2016)

48. Zhang, R.F., Li, M.C., Yin, H.M.: Rogue wave solutions and the bright and dark solitons of the (3+1)-dimensional Jimbo–Miwa equation. Nonlinear Dyn. **103**, 1071–1079 (2021)

49. Ma, W.X., Abdeljabbar, A., Asaad, M.G.: Wronskian and Grammian solutions to a (3+1)-dimensional generalized KP equation. Appl. Math. Comput. **217**, 10016–10023 (2011)

50. Wazwaz, A.M.: Multiple-soliton solutions for a (3+1)-dimensional generalized KP equation. Commun. Nonlinear Sci. Numer. Simul. **17**, 491–495 (2012)

51. Wazwaz, A.M., El-Tantawy, S.A.: A new (3+1)-dimensional generalized Kadomtsev–Petviashvili equation. Nonlinear Dyn. **84**, 1107–1112 (2016)

52. Jimbo, M., Miwa, T.: Solitons and infinite dimensional Lie algebras. Publ. Res. Inst. Math. Sci. **19**, 943–1001 (1983)

53. Clarkson, P.A., Mansfield, E.L.: On a shallow water wave equation. Nonlinearity **7**, 975–1000 (1994)

54. Tian, B., Gao, Y.T.: Beyond travelling waves: a new algorithm for solving nonlinear evolution equations. Comput. Phys. Commun. **95**, 139–142 (1996)

55. Zayed, E.M.E.: Traveling wave solutions for higher dimensional nonlinear evolution equations using the $(\frac{G'}{G})$-expansion method. J. Appl. Math. Inform. **28**, 383–395 (2010)

56. Tang, Y.N., Ma, W.X., Xu, W.: Grammian and Pfaffian solutions as well as Pfaffianization for a (3+1)-dimensional gen-

eralized shallow water equation. Chin. Phys. B **21**, 070212 (2012)

57. Zeng, Z.F., Liu, J.G., Nie, B.: Multiple-soliton solutions, soliton-type solutions and rational solutions for the (3+1)-dimensional generalized shallow water equation in oceans, estuaries and impoundments. Nonlinear Dyn. **86**, 667–675 (2016)

58. Liu, J.G., He, Y.: New periodic solitary wave solutions for the (3+1)-dimensional generalized shallow water equation. Nonlinear Dyn. **90**, 363–369 (2017)

59. Ablowitz, M.J., Satsuma, J.: Solitons and rational solutions of nonlinear evolution equations. J. Math. Phys. **19**, 2180–2186 (1978)

60. Rao, J., Porsezian, K., He, J.: Semi-rational solutions of the third-type Davey–Stewartson equation. Chaos **27**, 083115 (2017)

61. Rao, J., Cheng, Y., He, J.: Rational and semirational solutions of the nonlocal Davey–Stewartson equations. Stud. Appl. Math. **139**, 568–598 (2017)

62. Cao, Y., He, J., Mihalache, D.: Families of exact solutions of a new extended (2+1)-dimensional Boussinesq equation. Nonlinear Dyn. **91**, 2593–2605 (2018)

63. Cao, Y., Rao, J., Mihalache, D., He, J.: Semi-rational solutions for the (2+1)-dimensional nonlocal Fokas system. Appl. Math. Lett. **80**, 27–34 (2018)